Thickness effect on the microstructure, morphology and optoelectronic properties of ZnS films

2008 J. Phys.: Condens. Matter 20 035205

(http://iopscience.iop.org/0953-8984/20/3/035205)

J. Phys.: Condens. Matter **20** (2008) 035205 (10pp) doi:10.1088/0953-8984/20/03/035205

Thickness effect on the microstructure, morphology and optoelectronic properties of ZnS films

P Prathap[1], **N Revathi**[1], **Y P Venkata Subbaiah**[2] **and K T Ramakrishna Reddy**[1,3]

[1] Thin Films Laboratory, Department of Physics, Sri Venkateswara University, Tirupati-517 502, India
[2] Department of Physics, Yogi Vemana University, Kadapa-516 003, India

E-mail: ktrkreddy@hotmail.com

Received 2 July 2007, in final form 17 October 2007
Published 10 December 2007
Online at stacks.iop.org/JPhysCM/20/035205

Abstract

Thin films of ZnS with thicknesses ranging from 100 to 600 nm have been deposited on glass substrates by close spaced thermal evaporation. All the films were grown at the same deposition conditions except the deposition time. The effect of thickness on the physical properties of ZnS films has been studied. The experimental results indicated that the thickness affects the structure, lattice strain, surface morphology and optoelectronic properties of ZnS films significantly. The films deposited at a thickness of 100 nm showed hexagonal structure whereas films of thickness 300 nm or more showed cubic structure. However, coexistence of both cubic and hexagonal structures was observed in the films of 200 nm thickness. The surface roughness of the films showed an increasing trend at higher thicknesses of the films. A blue-shift in the energy band gap along with an intense UV emission band was observed with the decrease of film thickness, which are ascribed to the quantum confinement effect. The behaviour of optical constants such as refractive index and extinction coefficient were analysed. The variation of refractive index and extinction coefficient with thickness was explained on the basis of the contribution from the packing density of the layers. The electrical resistivity as well as the activation energy were evaluated and found to decrease with the increase of film thickness. The thickness had a significant influence on the optical band gap as well as the luminescence intensity.

(Some figures in this article are in colour only in the electronic version)

1. Introduction

In polycrystalline thin film devices, the performance and reliability will critically depend upon the microstructure, grain size and distribution, and defect density, that are in turn affected by deposition and post-deposition conditions as well as the thickness of the films. In recent years, various methods have been evolved to prepare smart materials and structures in thin film form that have a wide range of applications [1–3]. Generally in thin films, irrespective of the thin film deposition method used, stress could be developed due to the lattice and/or thermal expansion mismatch between the thin film and the supporting substrate. This stress can alter the mechanical as well as optoelectronic properties due to the distorted lattice and thus degrade the performance and life of the fabricated device [4]. Makino *et al* [5] reported that the stress could also induce the dark-line defects and piezoelectric effect in optoelectronic devices, that can reduce the operational lifetime and oscillator strength for excitonic transition. The developed lattice strain could be either compressional or tensile, which changes with the deposition temperature and thickness of the films and controls the mode of grain growth along with the surface morphology [6]. It has been reported recently that the structure and surface morphology changed with the film thickness, that alter the optical transmittance characteristics [7, 8] and other electronic properties [9, 10].

[3] Author to whom any correspondence should be addressed.

ZnS is a direct band gap semiconductor with two polymorphic structures, that has a wide band gap of 3.7 eV. Although there were extensive reports on the physical properties of ZnS films prepared by different methods [11–13], few reports are available on the thickness dependent physical properties of ZnS films, particularly on the change of photoluminescence with thickness in ZnS nanolayers. Valkonen *et al* reported the effect of thickness on the surface morphology of SILAR grown ZnS films on Si substrates [14]. Laukaitis *et al* studied the influence of thickness on structure, stress and morphology of SILAR grown ZnS films on GaAs substrates [15, 16]. In addition to this, various critical issues related to the optoelectronic properties of ZnS films as a function of thickness and the influence of residual strain on such properties need to be addressed in order to improve the performance of devices further making use of ZnS films. The high refractive index, wide energy band gap and high optical transmittance of ZnS films in the visible spectrum made this material a promising candidate in the area of optics to develop light reflectors [17] and dielectric filters [18]. Recently, it was also proved that ZnS films have potential in replacing the hazardous CdS as a buffer layer in solar photovoltaics [19]. This material exhibits different photoluminescent properties depending on the grain size and surface morphology [20–24]. It is therefore important to achieve a deeper understanding of the mechanical as well as the optoelectronic properties as a function of thickness for application of these layers in the fabrication of any new device.

In the present study, we have mainly focused our attention on thickness dependent physical properties of ZnS films, although the other deposition parameters like source stoichiometry, substrate temperature, source temperature, rate of evaporation and surface of the substrates used to grow the films can also equally influence the physical properties of the grown layers. In this context, we were successful in our earlier study in growing ZnS nanocrystalline layers by close spaced evaporation, a non-wet technique, wherein the substrate temperature and other deposition conditions have been optimized to prepare good quality layers by analysing the variation of microstructure and morphology of the films with growth temperature [25]. In this paper, we report on the dependence of microstructure, optoelectronic and photoluminescence properties on thickness of ZnS films grown by close spaced evaporation.

2. Experimental details

Thin films of ZnS were prepared by the close spaced evaporation (CSE) technique using a Hind Hi Vac Box Coater (model BC-300). In this method, the conventional thermal evaporation was modified such that the substrate was fixed at a distance of ∼5 cm from the source. The experimental arrangement of the CSE technique has been reported elsewhere [26]. ZnS films were deposited on ultrasonically cleaned Corning 7059 glass substrates by the evaporation of 5N pure ZnS powder, procured from Koch Chemicals, UK. The evaporant (ZnS) was placed in a molybdenum boat, which was used as an evaporation source and covered with a molybdenum sheet having small apertures to avoid bumping of the material during evaporation. The system was then pumped down to a base pressure of 5×10^{-6} mbar. The film thickness was controlled by a shutter placed between the source and substrate. The rate of deposition and thickness of the experimental films were monitored using the quartz crystal thickness monitor (model QTM-101) placed just below the substrate holder. The films were deposited in the thickness range of 100–600 nm at a deposition rate of 30 Å s^{-1} using a substrate temperature of 300 °C. The structural and morphological studies were carried out using a Siefert x-ray diffractometer (model 3003TT) and Vecco atomic force microscope, respectively. The elemental composition of the layers was studied using a VG Microtech ESCA2000 x-ray photoelectron spectrometer. The spectral transmittance of the films was recorded as a function of wavelength, that varied in the range 300–1500 nm, using a Hitachi U:3400 UV–vis–NIR spectrophotometer in order to determine the optical energy band gap, absorption coefficient, refractive index, packing density and extinction coefficient. The photoluminescence properties were studied using a fluorescence spectrophotometer (model Yvon Fluorolog 3). The electrical resistivity of the layers was measured using the two-probe method. Silver was used as electrodes for measuring the resistivity of the layers. The temperature dependence of electrical conductivity of the ZnS films was studied in the range 300–520 K.

3. Results and discussion

The visual observation of as-deposited films was uniform and pinhole free. The films were colourless at lower thickness and changed to whitish yellow colour with the increase of thickness. The layers were strongly adherent to the substrate and free from pinholes and visible cracks.

3.1. Compositional analysis

The elemental composition analysis of the as-grown layers with different thicknesses was determined using x-ray photoelectron spectrometric measurements. Figure 1 shows the typical XPS spectrum of ZnS layers of 300 nm thickness, recorded in the binding energy range 0–1200 eV. The XPS spectrum exhibited various peaks that correspond to the Zn $2p_{3/2}$, Zn $2p_{1/2}$ and S $2p_{3/2}$ at the binding energies of 1022, 1046 and 162.5 eV, respectively, in addition to the zinc Auger lines at 498 and 585 eV. The observed binding energy values are in good agreement with the reported data [13]. The evaluated areas under the Zn and S peaks gave a S/Zn ratio of ∼0.98. The XPS studies revealed that the S/Zn ratio in the layers increased from 0.93 to 0.99 with the increase of film thickness from 100 to 600 nm. The observed large sulfur deficiency in the 100 nm thick film might be due to either a thermal gradient between the substrate surface and deposited material or a lower sticking coefficient. This would ensure the re-evaporation of sulfur from the film surface due to the large difference in the vapour pressures of the constituent elements. These effects might be expected to minimize at higher thicknesses, where the incoming vapour flux would see the parent material as the substrate surface. Therefore, the ratio

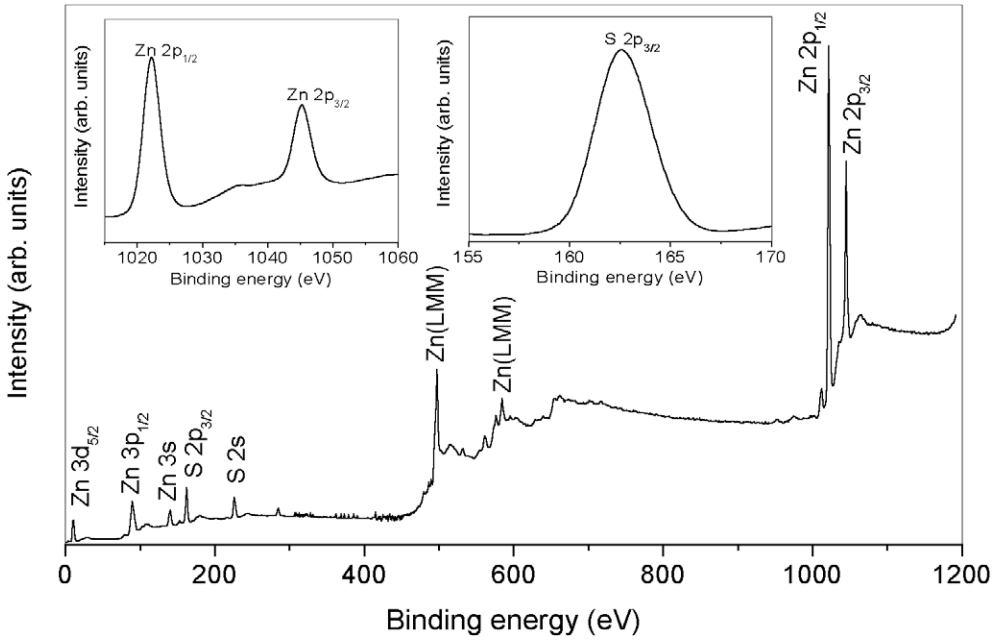

Figure 1. XPS spectrum of ZnS films grown with a thickness of 300 nm.

of S/Zn could reach a value of 0.99 for the films deposited at a thickness of 600 nm.

3.2. Structural studies

Figure 2 shows the x-ray diffractograms of ZnS films with different thicknesses. At a thickness of 100 nm, the films showed hexagonal structure with a prominent (100) orientation and the films deposited for a thickness of 200 nm showed the coexistence of both cubic and hexagonal structures with more amorphous background. With further increase of the film thickness, pure cubic structure was observed with a preferred (111) orientation. Therefore, these results indicated that the prevalence of the structure of ZnS films depends on the film thickness. Also some authors reported the presence of wurtzite structure for ZnS and also the coexistence of zinc-blende as well as wurtzite structures [27]. Johnston *et al* [28] and Cheng *et al* [29] reported the hexagonal structure, while Saratale *et al* [30] and Lee *et al* [31] reported the cubic structure for the films prepared by chemical bath deposition. Elidrissi *et al* reported that ZnS films grown by spray pyrolysis on glass substrates exhibited a mixture of both cubic and hexagonal phases [13]. This analysis shows that the presence of crystalline phase in ZnS films is highly sensitive to the method of preparation and the substrates used to prepare the layers.

Generally in polycrystalline thin film structures, the predominant structure or orientation mainly depends on the processing parameters. The structural changes occur by surface diffusion and migration of grain boundaries during the coalescence of two differently oriented nuclei. In such cases, smaller nuclei may easily rotate on coalescence, that induces the structural changes [32]. The various factors that influence the stable polycrystalline state of a material include the lowest surface energy, the grain boundary energy and the

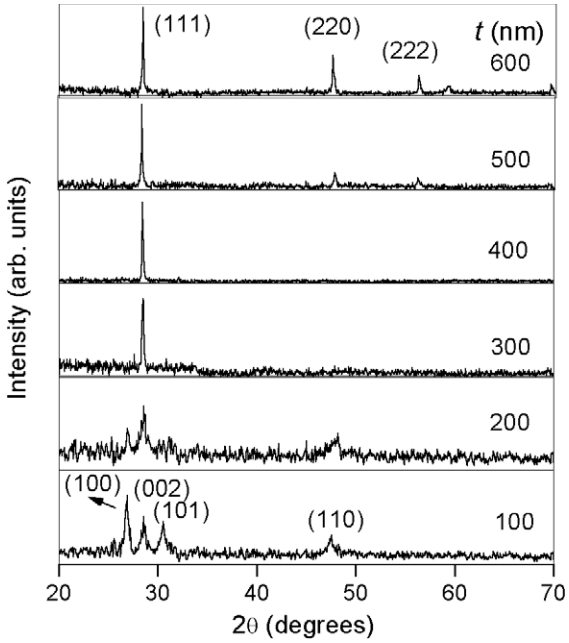

Figure 2. X-ray diffraction profiles of ZnS films.

diffusion of surface atoms [33]. The reports by Lee *et al* [34] reveal that the strain energy minimization and surface energy minimization would compete with one another to determine the preferred orientation of grain growth and the final texture of thin films. The extent of these energy states depends on the thickness of the films. The minimization of strain energy promotes one type of texture while the minimization of surface energy promotes another. Moreover, at a lower film thickness surface energy dominates, whereas at the higher film thickness strain energy will be significant. The surface structure of the

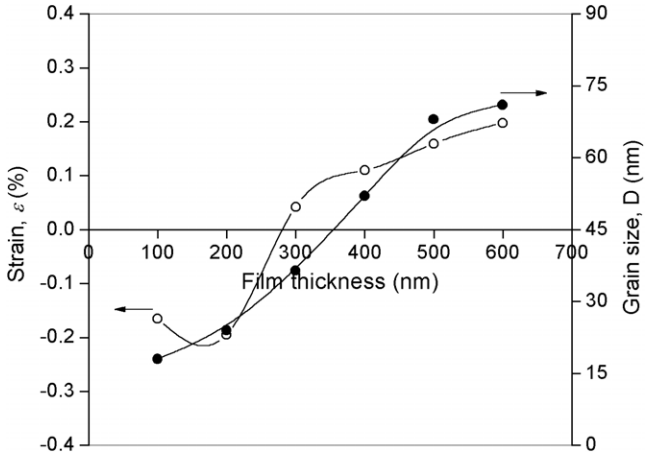

Figure 3. The variation of strain and grain size in the films with film thickness.

substrate forces the nuclei to grow along a specific orientation, preventing the nucleation along other orientations [35]. It can be concluded from the above discussion that the interaction at the film and substrate interface could be high at lower thickness values. This could cause the layers to grow in hexagonal structure. The influence of the substrate might be reduced with the increase of film thickness, as the deposited material could see the parent material as the substrate. For film thickness greater than 200 nm, all the layers showed only the (111) plane at 28.85° as the preferred orientation, corresponding to the zinc-blende type ZnS. A characteristic shift in the position of the diffraction peak was observed with the increase of film thickness, with a significant increase in the intensity of the (111) peak. Similar results were also reported by Mergel *et al* [36] in sputter deposited tin doped indium oxide films. This behaviour might be due to an improvement in the crystallinity with better crystallite size. However, at higher thicknesses other orientations such as (220), (112) and (002) were also observed in addition to the (111) orientation.

The evaluated lattice constants of the as-grown films differ from the bulk values ($a = 5.406$ Å for cubic, $a = 3.821$ Å, $c = 6.257$ Å for hexagonal). This indicates the presence of stress/strain in the as-deposited films, which might be caused by the defects, stoichiometric deviations and/or mismatch of thermal expansion coefficients of both the substrate and film. This can change the optoelectronic properties of the films due to the distorted lattice. The strain developed in the films with the film thickness was calculated using the relation [37]

$$\varepsilon = \frac{a - a_0}{a_0} \times 100\%, \tag{1}$$

where 'a' is the lattice constant of the ZnS film and a_0 is the unstrained bulk lattice parameter. Those films crystallized in hexagonal structure can exhibit variation in both the lattice constants, a and c. In the present case, we found that the variation of a was marginal and therefore the variation of c-axis length was considered in the determination of strain. The variation of strain with film thickness is shown in figure 3. It can be observed that the strain was compressional at lower thicknesses (<300 nm) whereas it was tensile at thicknesses of 300 nm or more. It is important to note that the higher compressional strain was observed at a film thickness of 200 nm, which could be due to the structural changes that took place in this critical thickness range. Tamulevicius *et al* [38] reported that the compressional strain could dominate in the two dimensional growth mode in SILAR grown CdS films. Therefore, the analysis of the present results indicated that the grain growth might be two dimensional due to the higher interaction between the film and substrate at thicknesses lower than 200 nm.

The crystallite size as a function of film thickness was evaluated using the Scherrer's equation [39] employing the full width at half maximum of the predominant peak and is shown in figure 3. The variation of grain size with film thickness showed the usual trend. At lower film thickness of 100 nm, the grain size was low (∼18.4 nm) and increased sharply to a value of 68.7 nm with the increase of film thickness to 500 nm. With further increase of film thickness, the improvement of the grain size saturated at 71.3 nm. The observed behaviour of grain size at lower thicknesses might be due to the stronger interaction between the substrate and vapour atoms, that restricts the mobility of both the ad-atoms and subcritical nuclei. As the film thickness increased, the effect of the substrate could be decreased, as the incoming vapour is being deposited on the initial layer itself, so that an increase in the grain size could be observed. At higher film thickness, the grain size reached a saturation value and the improvement was marginal.

3.3. Morphological studies

The AFM measurements were performed to analyse the surface topography of the as-grown layers. Figure 4 shows the surface morphology of ZnS films prepared for three different thicknesses, 100, 300 and 600 nm, scanned over the area of 1 μm × 1 μm. These pictures clearly showed the dependence of grain size as well as surface roughness on the film thickness. The AFM picture of the film grown for a thickness of 100 nm consisted of smaller crystallites that are uniformly distributed. These tend to grow three dimensionally with the increase of film thickness. The surface topographies of the films with thicknesses 100 and 200 nm showed a nearly similar structure. But at higher thicknesses, more than 400 nm, a significant improvement in the grain size took place. At the initial stages of the film growth, there were many nucleation centres present on the substrate surface. For a constant rate of deposition, the deposition time is very short for thinner films when compared to the thicker films. The small crystallites cannot grow into larger ones in thinner films due to the shorter deposition time, and hence the thinner films have small crystallites. With the increase of film thickness, coalescence of the small grains took place, leading to the formation of bigger crystallites in the film along with an improved crystallinity as observed from the XRD analysis. The grain size evaluated from AFM measurements varied in the range 19.4–72.1 nm with the increase of film thickness from 100 to 600 nm and nearly matched the grain size evaluated from the XRD measurements. The average surface roughness of the films increased from 1.5 to 2.4 nm

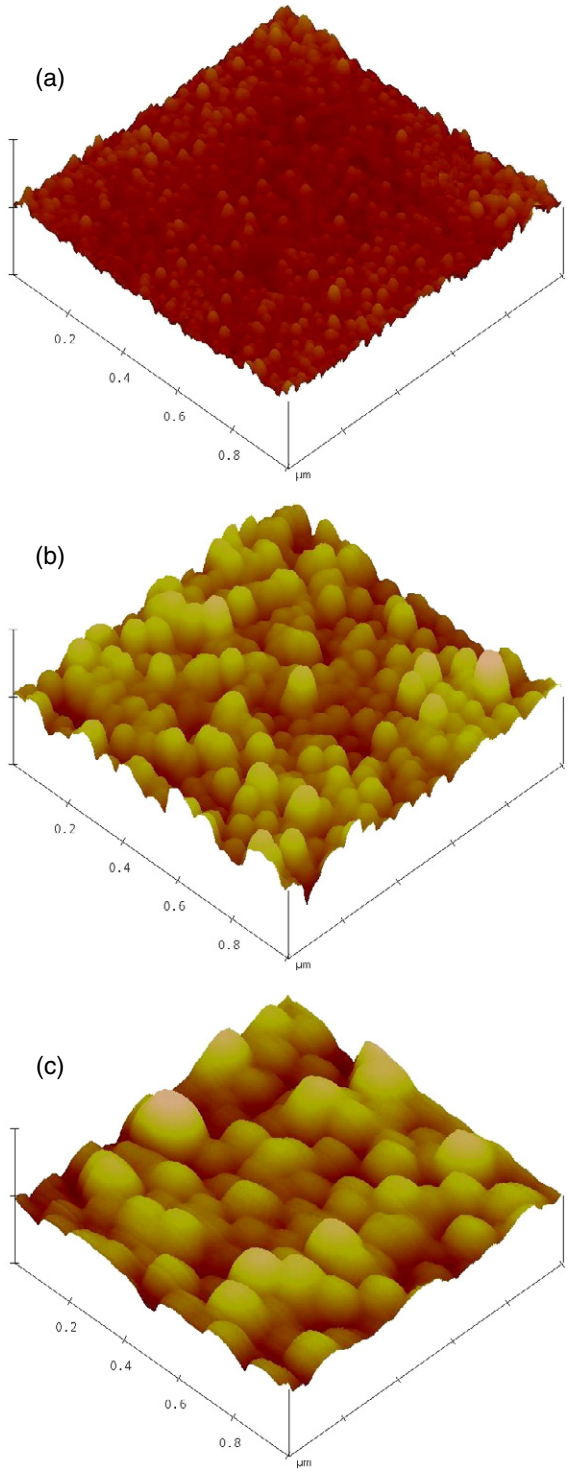

Figure 4. AFM pictures of ZnS films ((a) 100 nm; (b) 300 nm; (c) 600 nm).

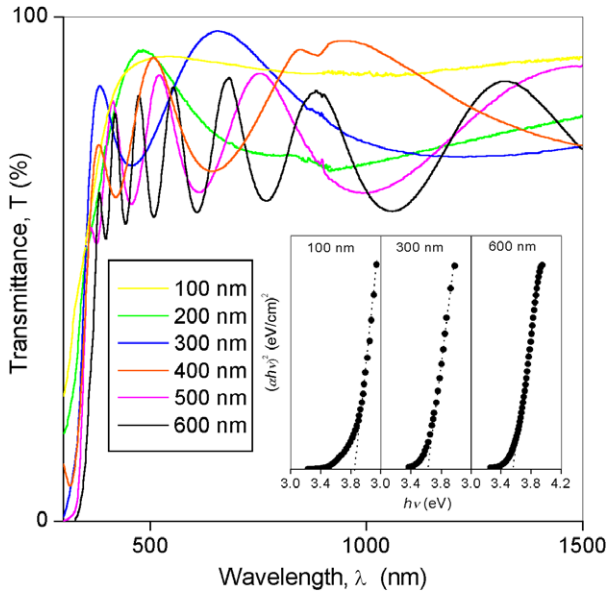

Figure 5. The change of optical transmittance with wavelength in ZnS layers.

when the film thickness varied in the range 100–400 nm. However, the surface roughness increased to 3.9 nm for the film thickness of 600 nm. The increase of roughness is associated with the increase of grain size. As the grains grew bigger, the density of grain boundaries decreased and the grain growth took place with a large variation in the height of the grains on the film surface. Therefore, it is apparent that the thickness of the film changes the grain size as well as the surface roughness. A similar increase of surface roughness with the increase of film thickness was also reported by Meng *et al* in sputtered indium tin oxide films [40].

3.4. Optical properties

Figure 5 shows the optical transmittance of the films recorded in the wavelength range 300–1500 nm. At lower film thickness, $t \sim 100$ nm, a high optical transmittance of ∼91% was observed, that decreased to 71% with further increase of film thickness up to 600 nm. The large decrease of transmittance at $t > 300$ nm could be due to the thickness effect, which is a common phenomenon observed in thin films. Figure 5 clearly indicates the blue-shift in the fundamental absorption edge with the decrease of film thickness. The absorption coefficient of all the films was found to be more than 10^4 cm^{-1}. Thinner films showed a slightly higher value when compared to the thicker films. Metin *et al* [41] also reported similar behaviour in chemical bath deposited CdS films and explained that the bigger sized grains leave a larger unfilled inter-granular volume so that the absorption per unit thickness is reduced. The type of optical transition and the energy band gap of the films was measured from the dependence of absorption coefficient, α, on the photon energy, $(h\nu)$. In the present case, the plot of $(\alpha h\nu)^2$ versus $(h\nu)$ is linear, indicating the direct band gap nature of the films, and extrapolating the linear portion of the curve onto the X-axis (inset of figure 5) gives the energy band gap of the films. The evaluated energy band gap varied from 3.85 to 3.54 eV with the change of thickness in the range 100–600 nm. The variation of energy band gap, E_g, as a function of lattice strain as well as thickness is shown in figure 6. The band gap was found to increase with the decrease of thickness. It is well known that the energy band gap of a semiconductor is affected by the residual strain, defects,

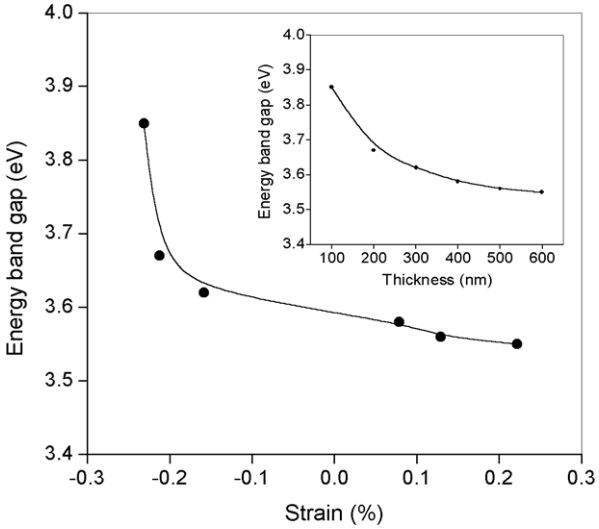

Figure 6. Variation of energy band gap with lattice strain; the inset shows the variation of energy band gap with the thickness of ZnS films.

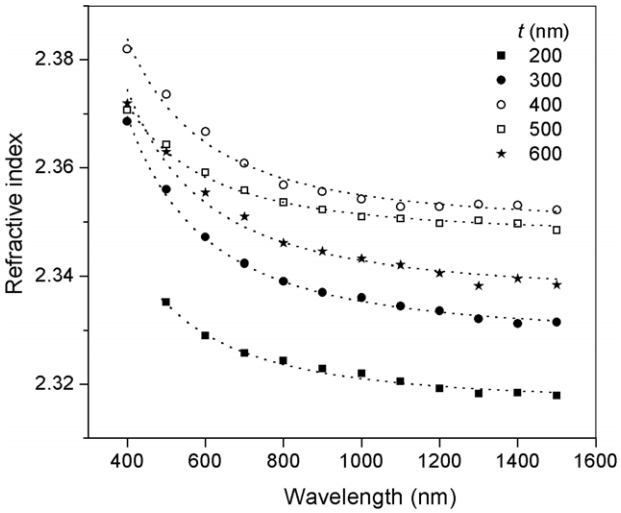

Figure 7. The dispersion spectra of the refractive index of ZnS films.

charged impurities, disorder at the grain boundaries [42] and also particle size confinement [43]. In addition, the tensile strain will result in a decrease of band gap due to the elongated lattice whereas a compressional strain increases the band gap due to the compressed lattice of the film [44, 45]. However, the particle size dependence might be dominant for the observed variation of the energy band gap with film thickness in the present study, where the band gap increased with the decrease of particle size.

The refractive index, n, for all the films deposited at a thickness $t \geqslant 200$ nm in the interference region was determined by the Swanepoel method using the relation [46]

$$n = [N + (N^2 - s^2)^{1/2}]^{1/2}, \tag{2}$$

where $N = 2sT + \frac{s^2+1}{2}$.

Here s is the refractive index of the substrate and $T = \frac{T_{\max} - T_{\min}}{T_{\max} \cdot T_{\min}}$.

Figure 7 shows the variation of refractive index with film thickness in the wavelength range 500–1500 nm. The results showed that the refractive index increased with the increase of film thickness from 200 to 400 nm and decreased again with the increase of thickness. The refractive index mainly depends on the density of the voids and their volume fraction, which are related to the packing density of the material. The initial increase of refractive index might be due to the close packing nature of the grains that results in the decrease of porous nature with the increase of film thickness as the coalescence of grains caused the densification of the layers. The films had the highest refractive index of 2.37 at a thickness of 400 nm. A decrease of refractive index was observed at film thickness $t > 400$ nm. This can be explained on the basis of the fact that as the grains grew bigger the grain boundaries would become less due to the size distribution of grains with the increase of film thickness, thereby changing the structure and morphology of the surface, leading to an improvement in the grain size. Further, these structural changes would lead to an increase of the volume fraction of the voids, which might be responsible for the reduction of the refractive index at higher film thickness. Hu *et al* also reported a similar behaviour for pulsed laser deposited HfO_2 films and explained that the increasing packing density would lead to higher refractive index in the films [47]. Moreover, it is interesting to note that in this investigation the films with compressional strain showed a lower value of refractive index while those having tensile strain showed higher values. This implies that the change of lattice constant would also influence the refractive index of the layers. Recently, some attention has been paid to monitoring the refractive index with the change of lattice constant. Mehan *et al* [48] reported that elongation of lattice constant would lead to an increase of the refractive index in rf-sputtered ZnO films, which supports our present results. In order to verify the effect of porosity or voids present in the films on the refractive index of the layers, the packing density, p, for the films with different film thicknesses was evaluated using the relation [49]

$$n_f^2 = \frac{(1-p)n_v^4 + (1+p)n_v^2 n_s^2}{(1+p)n_v^2 + (1-p)n_s^2}. \tag{3}$$

The variation of p with film thickness, as shown in figure 8, followed the behaviour of the refractive index. The packing density increases with the increase of thickness and reached a maximum value at a film thickness of 400 nm, that might be due to the significant reduction in the porosity. These results indicated the influence of both the lattice constant and packing density on the refractive index of the films.

The refractive index was found to decrease exponentially with the increase of wavelength from 500 to 1500 nm. The dispersion of refractive index data was fitted to the Cauchy relation [50]

$$n = a + b/\lambda^2, \tag{4}$$

where a and b are the Cauchy's parameters and λ is the wavelength of light used. Figure 7 shows the variation of refractive index with wavelength; the dotted curve represents the Cauchy fit for the equations given in table 1. This shows

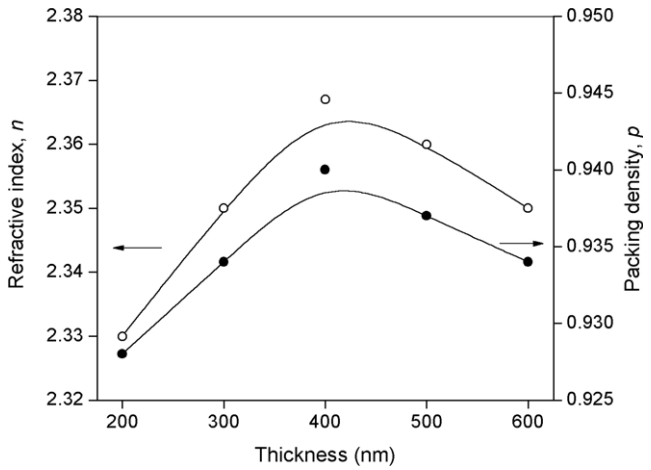

Figure 8. Refractive index and packing density as a function of film thickness.

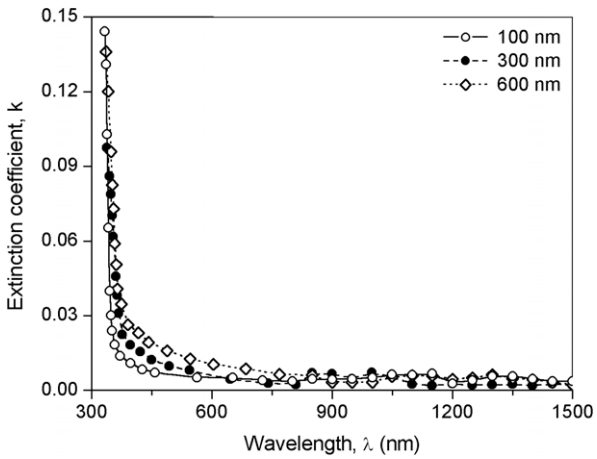

Figure 9. Extinction coefficient of ZnS layers as a function of wavelength.

Table 1. Cauchy's equations for different ZnS films.

S No	Film thickness (nm)	Cauchy relation, n
1	200	$2.3164 + 4638/\lambda^2$
2	300	$2.3288 + 6498/\lambda^2$
3	400	$2.3368 + 6019/\lambda^2$
4	500	$2.3494 + 5487/\lambda^2$
5	600	$2.3475 + 3886/\lambda^2$

that the films had normal dispersion for the entire wavelength range. These equations can be used to extrapolate to determine the refractive index in the strong absorption region where the interference fringes were absent.

The extinction coefficient (k) was directly calculated from the absorption coefficient by using the relation [46]

$$k = \frac{\alpha\lambda}{4\pi}. \tag{5}$$

The evaluated extinction coefficient had a maximum value near the absorption edge. The variation of extinction coefficient with wavelength in ZnS films that had different thicknesses is shown in figure 9. The value of extinction coefficient was found to be of the order of 10^{-2} and it increased with the increase of film thickness. The observed values of k for all the films grown in this study were slightly high, that might be due to the crystallographic defects such as grain boundaries and voids present in the layers. The slight increase of extinction coefficient at higher film thickness values might be due to the increase of optical scattering and optical loss that results from the increase of surface roughness [51].

3.5. Photoluminescence studies

The photoluminescence of ZnS is very complicated, as it depends on the preparation conditions, defects present, crystallite size and shape. The room temperature photoluminescence spectra of as-grown ZnS films were recorded with an excitation wavelength of 325 nm under identical conditions. The

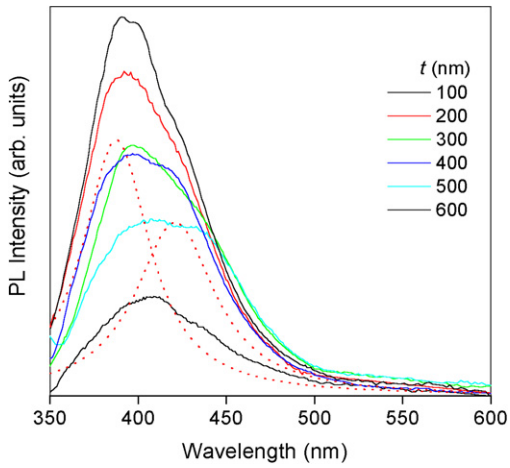

Figure 10. Photoluminescence spectra of ZnS films.

luminescence spectra, shown in figure 10, exhibited different luminescence intensities, with a blue-shift in the peak position with the decrease of film thickness. The luminescence peak was observed at an energy lower than the optical band gap for all the films, indicating the presence of impurity states in the mid-band-gap region. Several workers have attributed this type of luminescence to the emissions associated with the vacancy sites [52]. Semiconductor nanoparticles exhibit the luminescence from excitonic emissions as well as trapped emissions and the photoluminescence properties are limited by the large surface to volume ratio and surface defects of nanosized particles, which lead to the reduced excitonic emission via non-radiative surface recombination [53]. Hence, a few reports are available on the excitonic emission of ZnS nanoparticles due to the prevalence of trap-state emission [54–56]. The reports by Kumbhojkar *et al* [57] revealed that the red-shift observed in luminescence was caused by the deep hole trapped states arising from the dangling bonds at the crystal surface. Chen *et al* reported that only the trapped luminescence arising from the surface states can be observed in ZnS nanoparticles and this assumption was also supported by thermoluminescence measurements [58]. In order to get well defined band gap or excitonic

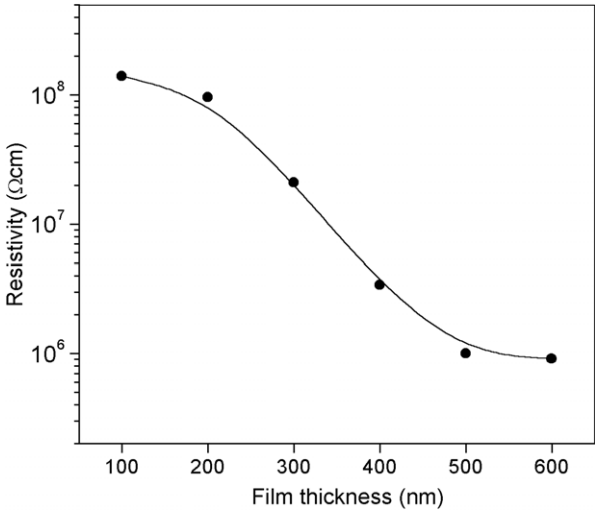

Figure 11. The change of electrical resistivity of ZnS layers with deposition rate.

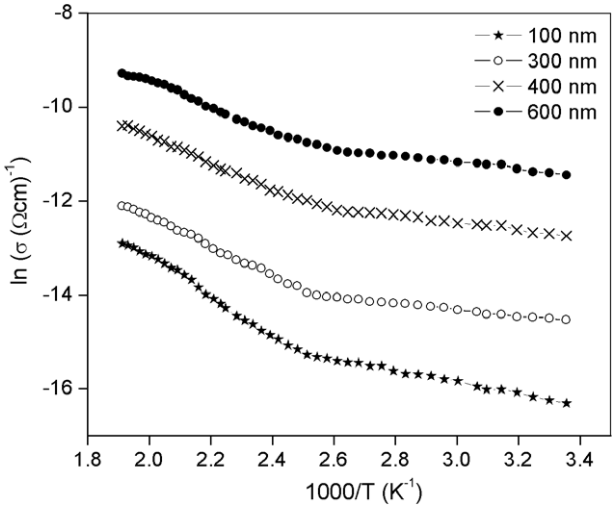

Figure 12. Electrical conductivities as a function of annealing temperature of ZnS films.

emission, it is essential to control the surface states. The density of these surface states increased with the decrease of crystallite size. This can reduce the probability of excitonic emission through the non-radiative surface recombination, leading to the appearance of a luminescence peak at energy lower than the band gap of the material. The de-convolution of the luminescence curves gave two emission peaks, located around 390 and 430 nm, depending on the nature of the transitions involved. The dotted curves in the plot show the de-convolution of the typical luminescence spectrum of the film deposited at a thickness of 200 nm. All the layers deposited at different thicknesses showed UV emission (PL_1) at 385.6, 387.4, 390.7, 391.8, 393.4 and 394.9 nm while other emissions (PL_2) also occurred at 416.3, 417.5, 423.2, 423.7, 436.9 and 437.1 nm, respectively. The observed blue-shift of the luminescence peak, PL_1, with the decrease of film thickness could be due to the increase of band gap with the film thickness. The luminescence peaks located around 390.7, 436.9 and 437.1 nm are associated with the zinc vacancies and the emissions located at 416.3 and 417.5 nm can be attributed to the interstitial sulfur [20, 59, 60]. The observed variation in the intensity of the luminescence clearly indicated the influence of surface area of the grains on the luminescence. It was reported that the luminescence intensity depends on the particle diameter [58, 59], where it increases with the increase of the density of surface states due to large surface to volume ratio for the smaller crystallites. Hence, the materials with smaller crystallites showed higher luminescence intensity compared to the crystallites of larger diameter.

3.6. Electrical properties

Figure 11 represents the dark resistivity of ZnS films measured at room temperature for different thicknesses. The resistivity showed a normal trend with the increase of film thickness. At lower thickness (100 nm) the films showed a high electrical resistivity of the order of 10^8 Ω cm, while at higher thickness (600 nm) the films had an electrical resistivity of 10^5 Ω cm. The decrease of resistivity can be attributed to the increase of grain size and the decrease of residual defects with film thickness [32]. This could also be supported by the variation of crystalline quality with the increase of film thickness as observed in the XRD analysis. It is interesting to note that at a film thickness of 200 nm a small increase of resistivity could be observed though the thickness is increased. At higher thickness, $t > 500$ nm, the rate of decrease of resistivity is marginal. This might be due to the saturation of the grain size at higher thicknesses. The temperature dependent conductivity measurements were made on the films deposited for different film thicknesses in order to evaluate the activation energy of the charge carriers. Figure 12 shows the plots of conductivity versus temperature for four typical thicknesses measured in the temperature range 300–520 K. The conductivity plots showed two distinct regions with the increase of temperature, that were also observed in other II–VI compounds [61, 62]. The conductivity increased slowly in the low temperature region (300–390 K) whereas an abrupt increase was observed in the high temperature region (390–520 K). The activation energy of the charge carriers was calculated using the relation

$$\sigma = \sigma_0 \exp(-\Delta E / K T_a), \tag{6}$$

where σ is the conductivity, ΔE the activation energy and T_a the annealing temperature. The estimated activation energies, E_1 and E_2, varied in the range 0.61–0.28 and 0.14–0.06 eV in the high and low temperature zones, respectively. The activation energy values evaluated in the high temperature region for the films of higher thickness closely matched with the data reported by Gupta *et al* for ZnS_xSe_{1-x} films grown by the hot wall technique [58]. This can be attributed to the stacking disorder of the grains as the films were deposited on amorphous substrates [63]. In general, the electrical resistivity and activation energy of the charge carriers are mainly influenced by the presence of native defects such as Zn interstitials and S vacancies, which cause an increase of shallow donor levels. Moreover, the electron transport

properties are affected by the high density of defects such as dislocations, stacking faults, microtwins etc, which are inherent in the growth process of thin films [32] and the crystallinity of the grains [64]. The observed higher activation energy in both the high and low temperature regions for the films with lower thickness might be due to the poor crystallinity of the grains, whereas the lower resistivity and activation energy observed in the thicker films could be due to the good connectivity of the grains with better crystallite size. However, a deviation from the normal trend in the resistivity as well as activation energy could be observed at a film thickness of the order of 200 nm. This might be due to the higher degree of structural disorder induced by the coexistence of cubic and hexagonal structures as observed from the structural analysis.

4. Conclusions

Highly crystalline cubic ZnS films have been deposited by simple close spaced evaporation at a substrate temperature of 300 °C with different thicknesses. The influence of film thickness on the structural, morphological, optical and electrical properties was found to be significant. A change in the structure from hexagonal to cubic form was observed with the increase of film thickness along with an improvement in the crystalline quality of the layers. The surface roughness increased with the increase of film thickness while the optical band gap decreased from 3.84 to 3.54 eV with the increase of film thickness from 100 to 600 nm. The photoluminescence spectra of the as-grown layers exhibited closely separated doublet structures, indicating that the transitions involve the localized states in the band gap region, which arise from the defects present in the layers. A highest luminescence intensity was observed for the films grown at a thickness of 100 nm. ZnS films with lower thickness had the higher electrical resistivity of 10^8 Ω cm, that decreased to 10^5 Ω cm with the increase of film thickness to 600 nm.

References

[1] Zhao Z W, Tay B K, Chen J S, Hu J F, Sun X W and Tan S T 2005 *Appl. Phys. Lett.* **87** 251912
[2] Yin L W, Bando Y, Zhan J H, Li M S and Golberg D 2005 *Adv. Mater.* **17** 1972
[3] Ong H C, Zhu A X E and Du G T 2002 *Appl. Phys. Lett.* **80** 941
[4] Zhao D G, Xu S J, Xie M, Tong S Y and Yang H 2003 *Appl. Phys. Lett.* **83** 677
[5] Makino T, Yasuda T, Segawa Y, Ohtomo A, Tamura K, Kawasaki M and Koinuma H 2001 *Appl. Phys. Lett.* **79** 1282
[6] Tersoff J, Teichert C and Lagally M G 1996 *Phys. Rev. Lett.* **76** 1675
[7] Lai F, Li M, Wang H, Hu H, Wang X, Hou J G, Song Y and Jiang Y 2005 *Thin Solid Films* **488** 314
[8] Bruggemann R, Reinig P and Holling M 2003 *Thin Solid Films* **427** 358
[9] Kim H, Horwitz J S, Kushto G, Pique A, Karafi Z H and Gilmore C M 2000 *J. Appl. Phys.* **88** 6021
[10] Qiao Z, Latz R and Mergel D 2004 *Thin Solid Films* **466** 250
[11] Antony A, Murali K V, Manoj R and Jayaraj M K 2005 *Mater. Chem. Phys.* **90** 106
[12] Shao L X, Chang K H and Hwang H L 2003 *Appl. Surf. Sci.* **212/213** 305
[13] Elidrissi B, Addou M, Regragui M, Bougrine A, Akchouane A and Bernede J C 2001 *Mater. Chem. Phys.* **68** 175
[14] Valkonen M P, Lindroos S, Resch R, Leskela M, Friedbacher G and Grasserbauer M 1998 *Appl. Surf. Sci.* **136** 131
[15] Laukaitis G, Lindroos S, Tamulevicius S, Leskela M and Rackaitis M 2000 *Mater. Sci. Eng.* A **288** 223
[16] Laukaitis G, Lindroos S, Tamulevicius S and Leskela M 2001 *Appl. Surf. Sci.* **185** 134
[17] Ruffner J A, Hilmel M D, Mizrahi V, Stegeman G I and Gibson U 1989 *Appl. Opt.* **28** 5209
[18] Ledger A M 1979 *Appl. Opt.* **18** 2979
[19] Rusu M, Eisele W, Wurz R, Ennaoui A, Lux-Steiner M Ch, Niesen T P and Karg F 2003 *J. Phys. Chem. Solids* **64** 2037
[20] Denzler D, Olschewski M and Sattler K 1998 *J. Appl. Phys.* **84** 2841
[21] Ghosh S, Mukherjee A, Kim H and Lee C 2003 *Mater. Chem. Phys.* **78** 726
[22] Lu H Y, Chu S Y and Tan S S 2004 *J. Cryst. Growth* **269** 385
[23] Zhang X, Song H, Yu L, Wang T, Ren X, Kong X, Xie Y and Wang X 2006 *J. Lumin.* **118** 251
[24] Ye C, Fang X, Li G and Zhang L 2004 *Appl. Phys. Lett.* **85** 3035
[25] Subbaiah Y P V, Prathap P and Reddy K T R 2006 *Appl. Surf. Sci.* **253** 2409
[26] Subbaiah Y P V, Prathap P, Devika M and Reddy K T R 2005 *Physica* B **365** 240
[27] Hichou A El, Addou M, Bubendorff J L, Ebothe J, Idrissi B El and Troyon M 2004 *Semicond. Sci. Technol.* **19** 230
[28] Johnston D A, Carletto M H, Reddy K T R, Forbes I and Miles R W 2002 *Thin Solid Films* **403** 102
[29] Cheng J, Fan D B, Wang H, Liu B W, Zhang Y C and Yan H 2003 *Semicond. Sci. Technol.* **18** 676
[30] Saratale S D, Sankapal B R, lux-Steiner M and Ennaoui A 2005 *Thin Solid Fillms* **480** 168
[31] Lee J, Lee S, Cho S, Kim S, Park I Y and Choi Y D 2002 *Mater. Chem. Phys.* **77** 254
[32] Chopra K L 1969 *Thin Film Phenomena* (New York: McGraw-Hill)
[33] Fujihara S, Sasaki C and Kimura T 2001 *Appl. Surf. Sci.* **180** 341
[34] Lee D N 2003 *Thin Solid Films* **434** 183
[35] Nikolic L M, Radonjic L and Srdic V V 2005 *Ceram. Int.* **31** 261
[36] Mergel D, Stass W, Ehl G and Barthel D 2000 *J. Appl. Phys.* **88** 2437
[37] Ong H C, Zhu A X E and Du G T 2002 *Appl. Phys. Lett.* **80** 941
[38] Tamulevicius S, Valkonen M P, Laukaitis G, Lindroos S and Leskela M 1999 *Thin Solid Films* **355/356** 430
[39] Warren B E 1990 *X-ray Diffraction* (New York: Dover) p 253
[40] Meng L J and dos Santos M P 1997 *Thin Solid Films* **303** 151
[41] Metin H and Esen R 2003 *J. Cryst. Growth* **258** 141
[42] Dow J D and Redfield D 1972 *Phys. Rev.* B **5** 594
[43] Wang Y G, Lau S P, Lee H W, Yu S F, Tay B K, Zhang X H and Hng H H 2003 *J. Appl. Phys.* **94** 354
[44] Yao T, Okada Y, Matsui S, Ischida K and Fujimoto I 1987 *J. Cryst. Growth* **81** 518
[45] Zhao D G, Xu S J, Xie M H, Tong S Y and Yang H 2003 *Appl. Phys. Lett.* **83** 677
[46] Swanepoel R 1983 *J. Phys. E: Sci. Instrum.* **16** 1214
[47] Hu H, Zhu C, Lu Y F, Wu Y H, Liew T, Li M F, Cho B J, Choi W K and Yakovlev N 2003 *J. Appl. Phys.* **94** 551
[48] Mehan N, Gupta V, Sreenivas K and Mansingh A 2004 *J. Appl. Phys.* **96** 3134
[49] Harris M, Macleod H A and Ogura S 1979 *Thin Solid Films* **57** 173
[50] Modreanu M, Gartner M, Tomozeiu N and Szekeres A 2001 *J. Optoelectron. Adv. Mater.* **3** 575

[51] Lai F, Li M, Wang H, Hu H, Wang X, Hou J G, Song Y and Jiang Y 2005 *Thin Solid Films* **488** 314
[52] Zhang X, Song H, Yu L, Wang T, Ren X, Kong X, Xie Y and Wang X 2006 *J. Lumin.* **118** 251
[53] Chen W, Wang Z, Lin Z and Lin L 1997 *Appl. Phys. Lett.* **70** 1465
[54] Zhang Z Z, Shen D Z, Zhang J Y, Shan C C, Lu Y M, Liu Y C, Li B H, Zhao D X, Yao B and Fan X W 2006 *Thin Solid Films* **513** 114
[55] Jiang Y, Meng X M, Liu J, Hong Z R, Lee C S and Lee S T 2003 *Adv. Mater.* **15** 1195
[56] Wageh S, Zhao S L and Xu X R 2003 *J. Cryst. Growth* **255** 332
[57] Kumbhojkar N, Nikesh V V and Kshirsagar A 2000 *J. Appl. Phys.* **88** 6260
[58] Chen W, Wang Z, Lin Z and Lin L 1997 *Appl. Phys. Lett.* **70** 1465
[59] Lu H Y, Chu S Y and Tan S S 2004 *J. Cryst. Growth* **269** 385
[60] Becker W G and Bard A J 1983 *J. Phys. Chem.* **87** 4888
[61] Morales R L, Falfan M R, Moreno O P, Alvarez J P, Cabrera R H, Flores C A, Angel O Z, Mandujano O G, del Angel P, Montes J L M and Lopez L B 1999 *J. Electrochem. Soc.* **146** 2546
[62] Rusu G I, Popa M E, Rusu G G and Salaoru I 2003 *Appl. Surf. Sci.* **218** 222
[63] Gupta P, Bhattacharyya D, Chaudhuri S and Pal A K 1992 *Thin Solid Films* **221** 154
[64] Kale R B and Lokhande C D 2004 *Appl. Surf. Sci.* **223** 343